

ORIGINAL PRE-CLINICAL SCIENCE

Epicardial transplantation of atrial appendage micrograft patch salvages myocardium after infarction



Xie Yanbo, MD,^{a,1} Milla Lampinen, PhD,^{b,1} Juuso Takala, BM,^{b,1}
Vilbert Sikorski, BM,^{b,1} Rabah Soliymani, MSc,^{c,d} Miikka Tarkia, PhD,^b
Maciej Lalowski, PhD,^{c,d} Eero Mervaala, MD, PhD,^b Markku Kupari, MD, PhD,^e
Zhe Zheng, MD, PhD,^a Shengshou Hu, MD, PhD,^a Ari Harjula, MD, PhD,^e and
Esko Kankuri, MD, PhD^b, on behalf of the AADC consortium

From the ^aState Key Laboratory of Cardiovascular Disease, Fuwai Hospital, National Center for Cardiovascular Diseases, Chinese Academy of Medical Sciences and Peking Union Medical College, Beijing, China; ^bDepartment of Pharmacology, Faculty of Medicine, University of Helsinki, Helsinki, Finland; ^cDepartment of Biochemistry and Developmental Biology, Faculty of Medicine, University of Helsinki, Helsinki, Finland; ^dHelsinki Institute of Life Science (HiLIFE), University of Helsinki, Helsinki, Finland; and the ^eHeart and Lung Center, Helsinki Central Hospital and University of Helsinki, Helsinki, Finland.

KEYWORDS:

cell therapy;
myocardial infarction;
heart failure;
myocardial
regeneration;
atrial appendage;
site-selective
proteomics

BACKGROUND: Ischemic heart disease remains the leading cause of mortality and morbidity worldwide despite improved possibilities in medical care. Alongside interventional therapies, such as coronary artery bypass grafting, adjuvant tissue-engineered and cell-based treatments can provide regenerative improvement. Unfortunately, most of these advanced approaches require multiple lengthy and costly preparation stages without delivering significant clinical benefits.

METHODS: We evaluated the effect of epicardially delivered minute pieces of atrial appendage tissue material, defined as atrial appendage micrografts (AAMs), in a mouse myocardial infarction model. An extracellular matrix patch was used to cover and fix the AAMs onto the surface of the infarcted heart.

RESULTS: The matrix-covered AAMs salvaged the heart from the infarction-induced loss of functional myocardium and attenuated scarring. Site-selective proteomics of injured ischemic and uninjured distal myocardium from AAMs-treated and -untreated tissue sections revealed increased expression of several cardiac regeneration-associated proteins (i.e., periostin, transglutaminases, and glutathione peroxidases) and activation of pathways responsible for angiogenesis and cardiogenesis in relation to AAMs therapy.

CONCLUSIONS: Epicardial delivery of AAMs encased in an extracellular matrix patch scaffold salvages functional cardiac tissue from ischemic injury and restricts fibrosis after myocardial infarction. Our results support the use of AAMs as tissue-based therapy adjuvants for salvaging the ischemic myocardium.

J Heart Lung Transplant 2020;39:707–718

© 2020 The Author(s). Published by Elsevier Inc. on behalf of International Society for Heart and Lung Transplantation. This is an open access article under the CC BY-NC-ND license.

(<http://creativecommons.org/licenses/by-nc-nd/4.0/>)

¹These authors have contributed equally to this work.

Reprint requests: Esko Kankuri, MD, PhD, Department of Pharmacology, Faculty of Medicine, University of Helsinki, Haartmaninkatu 8, PO Box 63,

FIN-00014, Finland. Telephone: +358-29-41-25336. Fax: +358-2941-25364.

E-mail address: esko.kankuri@helsinki.fi

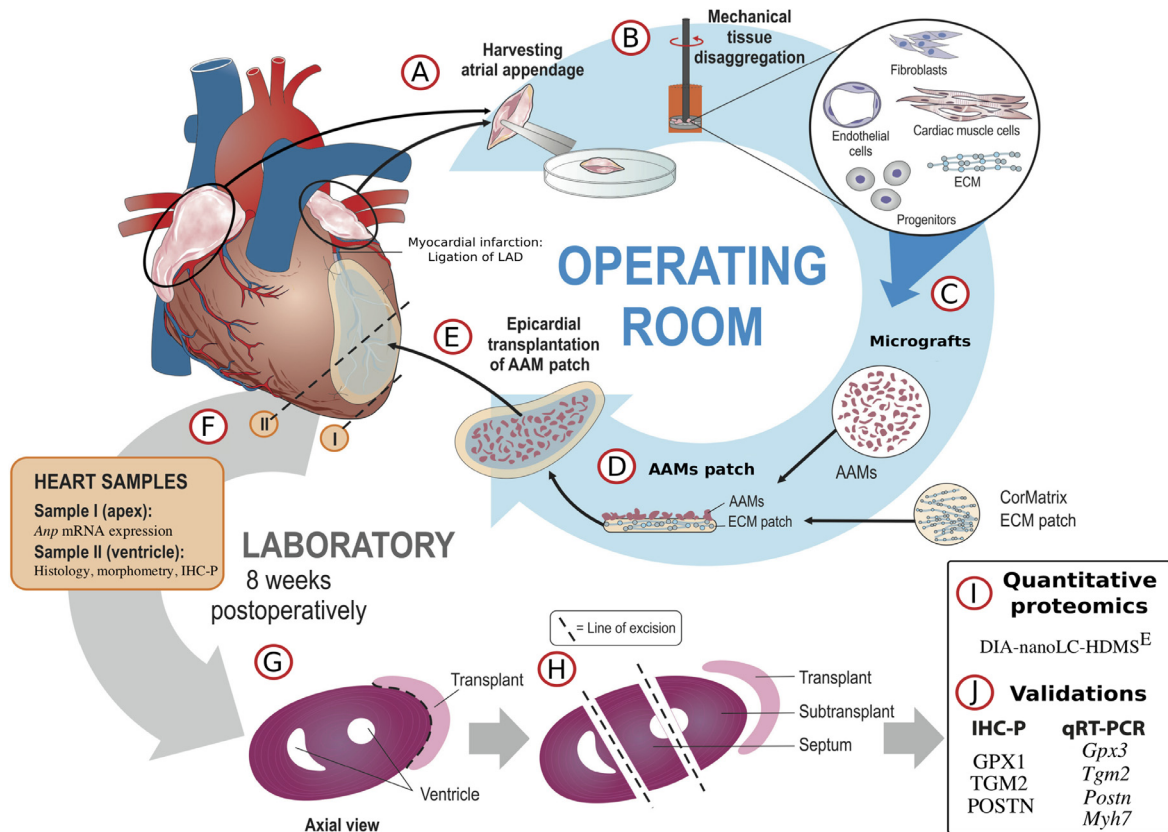


Figure 1 Overview of the study protocol. A schematic presentation of the processes carried out in the operating room and subsequently, in the laboratory are illustrated. For further information, see the detailed Materials and Methods in Supplementary Materials and Methods available online. (A) For each AAMs patch, both left and right atrial appendages were harvested from 3 syngeneic donor mice after placement of an atrial clip. (B, C) Harvested appendages were disaggregated to AAMs with a Rigenera machine. (D) An ECM sheet (CorMatrix ECM for cardiac tissue repair) was peeled into 4 layers, and 1-ply sheets were cut into circles using an 8-mm-diameter tissue punch. To create an AAMs patch, we evenly dispersed the AAMs suspension containing tissue material from 6 appendages (3 from each of the right and left sides) onto the matrix sheet and sealed it with a thin layer (10 μ l volume) of fibrin tissue glue. (E) The AAMs patch was subsequently fitted onto the recipient's heart with the AAMs-containing side facing the epicardium of the left ventricle at the site of infarction. The transplant was further fixed to the myocardium by 3 sutures to ensure that the patches remained in place. (F) After the 8-week follow-up, the animals were sacrificed, their hearts were excised, and the ventricle tissue samples were collected for histology or snap-frozen in liquid nitrogen. Apices were also collected for the measurement of *Anp* mRNA expression with qRT-PCR. (G) Thin histological sections were used for immunohistochemistry and morphometry. (H, I) Cryosections of 12 μ m thickness were collected from 3 anatomic groups (transplant/patch, sub-transplant, and septum) for proteomic profiling. (J) Lastly, the rest of the cryopreserved samples were used for selected validating qRT-PCR measurements and paraffin-embedded tissue samples for IHC-P staining. AAMs, atrial appendage micrografts; *Anp*, atrial natriuretic peptide; ECM, extracellular matrix; IHC-P, immunohistochemistry on paraffin-embedded tissues; qRT-PCR, quantitative real-time reverse transcription polymerase chain reaction.

Ischemic heart disease has persistently maintained its rank as the global leading cause of mortality.¹ Replacement of functional myocardium with a non-contractile fibrotic scar after irreversible ischemic injury overactivates compensatory mechanisms and contributes to myocardial rigidity and eventually, to the development of heart failure (HF) over time.² Therapeutic interventions alleviate symptoms but fail to restore lost myocardial tissue.^{3,4} Regenerative tissue engineering and cell-based therapies have been suggested to directly or indirectly instigate recovery of tissue function. Many cell-based therapies have poor clinical translatability owing to high complexity, costs, lengthy preparation times, requirements for special production facilities, and sometimes frank incompatibility with clinical practice.^{5,6} Although a plethora of cell types have been

evaluated in clinical trials, none are used as a part of clinical practice.⁷

Studies conducted with cardiac progenitor cells stimulated further interest in functional heart regeneration.^{8,9} Unfortunately, some of these studies were associated with major controversies, and the cardiac cell therapy community entered a state of disbelief. The autologous atrial appendages have an immunologically favorable cardiac origin, and together with findings indicating that atrial appendages harbor a rich cardiac progenitor cell pool^{10–12} these characteristics support the use of atrial appendage tissue as a cardiac cell-based therapy adjuvant.¹³ The atrial appendage-derived cells consortium recently demonstrated clinical feasibility of intraoperative processing and epicardial transplantation of autologous atrial appendage micrografts (AAMs).^{14,15}

In this study, we investigated the functional efficacy and molecular therapeutic mechanisms of epicardial AAMs patch transplantation in a murine model of myocardial infarction (MI) and HF (Figure 1).

Methods

A full-length description of the methods is available online as a Supplementary Material (as detailed Materials and Methods) at www.jhltonline.org. Figure 1 summarizes the study protocol. A brief overview of the methods is presented here.

Both atrial appendages were harvested and processed to AAMs from 3 male donor mice for each syngeneic transplant (42 mice in total). A total of 40 age-matched male mice (inbred 129 × 1/SvJ mice, JAX stock #000691, the Jackson Laboratory, Bar Harbor, ME) were divided into the following groups: Sham-operated (Sham group, *n* = 4); left anterior descending artery (LAD) ligation to induce MI (MI group, *n* = 9); LAD ligation followed by epicardial transplantation of extracellular matrix (ECM) patch without AAMs (ECM patch group, *n* = 13); and LAD ligation followed by an AAMs patch, an ECM patch with AAMs, and transplantation (AAMs patch group, *n* = 14). Cardiac function was evaluated weekly by echocardiography (ECHO), and after an 8-week follow-up, the animals were sacrificed and their hearts collected for analyses, including (1) atrial natriuretic peptide gene expression with quantitative real-time reverse transcription polymerase chain reaction from heart apices; (2) ventricular morphometric assessment with wall thickness, scar transmural, and planimetric measurements; and (3) histological evaluation for myocardial preservation with antibody and picrosirius red stain against cardiac troponin T

(cTnT) and collagens, respectively. Collagen staining was further supplemented with microscopy using circularly polarized light to sub-type mature (Type I) and immature (Type III) collagens.

Another set of mice was used to evaluate the mechanisms of AAMs. Male mice (strain 129 × 1/SvJ) were divided into 3 groups to receive either epicardial ECM (*n* = 7) or AAMs (*n* = 7) patch therapies after MI or Sham control (*n* = 4). As previously described, the animals were sacrificed, their hearts were collected, but in this study cryopreserved after the 8-week follow-up. Transplant, sub-transplant, and remote septal tissue samples were dissected from thin cryosections and subsequently processed for label-free site-targeted proteomic analysis (DIA-nanoLC-HD-MS^E; AAMs patch, *n* = 4 × 3; ECM patch, *n* = 4 × 3). Before bioinformatic analyses using Ingenuity Pathway Analysis software, the proteomic data were scrutinized by principal component analysis by Spearman correlation heatmap, resulting in the exclusion of outliers. The results were validated using antibody staining on tissues (targeting periostin [POSTN], transglutaminase 2 [TGM2], and glutathione peroxidase [GPX1] proteins) and by quantitative real-time reverse transcription polymerase chain reaction assaying *Postn*, *Tgm2*, *Gpx3*, and *Myh7* mRNA transcripts. The proteomics data have been deposited to the mass spectrometry interactive virtual environment as data set MSV000084120.

Results

Myocardial function

Left ventricular ejection fraction (LVEF) and area under the curve (AUC) analyses spanning the 8-week follow-up

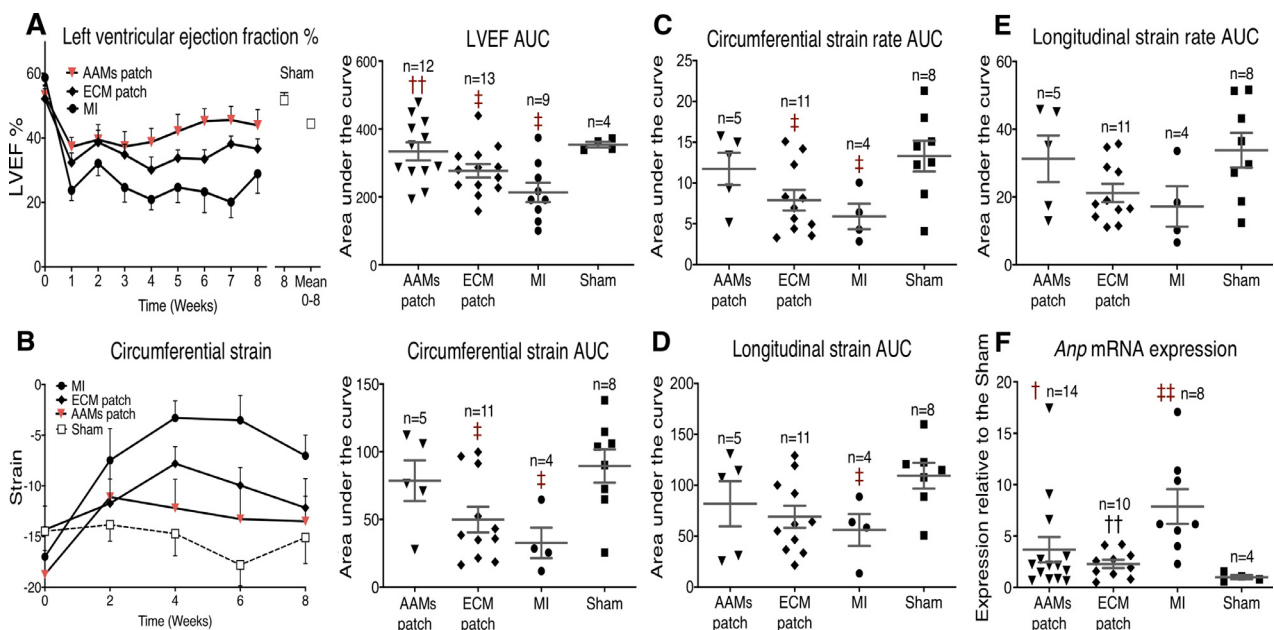


Figure 2 Myocardial function. (A) The left panel shows weekly performed LVEF measurements and the right panel shows AUC analysis from the LVEF follow-up data. (B) The left panel shows the circumferential strain measured with ECHO at 2-week intervals, whereas the right panel shows the corresponding AUC. (C) AUC analysis of the circumferential strain rate. (D) AUC analysis of the longitudinal strain. (E) AUC analysis of the longitudinal strain rate. (F) Relative expression of *Anp* mRNA to the expression of 18S mRNA from apex tissue samples as analyzed by real-time PCR. *†/‡ *p* < 0.05, **††/‡‡ *p* < 0.01, ***†††/‡‡‡ *p* < 0.001; *, *p*-value vs the ECM patch group; †, *p*-value vs the MI group; ‡, *p*-value vs Sham group. Two-tailed Mann-Whitney *t*-test was applied, and data normality assessed with the Shapiro-Wilk test for normality. The scatter plot data represent mean ± SEM. The *n*-values represent separate mice measured with high confidence and regarding *Anp* mRNA expression, number of analyzed heart apices. *Anp*, atrial natriuretic peptide; AUC, area under the curve; ECHO, echocardiography; LVEF, left ventricular ejection fraction; PCR, polymerase chain reaction; SEM, standard error of the mean.

period are presented in [Figure 2A](#). ECHO recordings demonstrated improved functional recovery in the AAMs patch group compared with those in the extracellular matrix (ECM) patch and MI groups. Lower-initial LVEF values in the Sham group were as a result of the lower weight of the group's mice at the beginning of the experiment.

In all intervention groups, LVEF decline was evident during the first 2 weeks of the follow-up. The acute declines in LVEF at 1-week time-point post-operatively in AAMs patch, ECM patch, and MI groups were $18.03 (54.49 \pm 2.93\% - 36.69 \pm 2.56\%)$, $19.77 (52.15 \pm 3.10\% - 32.38 \pm 2.96\%)$, and $34.94 (58.72 \pm 2.58\% - 23.78 \pm 3.16\%)$ percentage points, respectively, with a significant difference between AAMs patch and MI groups. In the later phase of the follow-up, the LVEF curves of the AAMs and ECM patch groups separated, suggesting a prolonged therapeutic effect from the AAMs. Significantly higher mean LVEF values were observed in the AAMs group than in the MI group from the fourth week onward until the seventh week of follow-up. The [Supplementary Table S1](#) (refer to [Supplementary Material Table S1](#) available online at www.jhltonline.org) provides the values of all ECHO parameters.

[Figure 2A](#) shows the LVEF measurements and AUC analysis over the entire follow-up period. The AAMs patch group demonstrated a highly preserved LVEF function compared with the MI group. The average LVEF AUC values were 334.2 ± 26.68 (AAMs patch), 277.1 ± 19.85 (ECM patch), 213.4 ± 28.55 (MI), and 354 ± 8.21 (Sham).

The functional state of the left ventricle was further assessed by strain analyses. AUC data are presented in [Figure 2B–E](#) and the complete data on strain analyses are available as [Supplementary Material \(Supplementary Material Figure S1 and Table S1 online\)](#). Overall, strain parameters in both patch groups were well-preserved, with the greatest preservation in the AAMs patch group.

Mean circumferential strain values ([Figure 2B](#)) at the 8-week time-point were -13.5 ± 2.48 (AAMs patch), -12.2 ± 2.87 (ECM patch), -7.0 ± 2.04 (MI), and -15.1 ± 2.57 (Sham). AUC analysis ([Figure 2B](#)) showed a preserved function only in the AAMs patch group. The average AUC values for circumferential strain were 78.6 ± 15.04 (AAMs patch), 49.9 ± 9.50 (ECM patch), 32.6 ± 11.27 (MI), and 89.46 ± 12.30 (Sham). Mean circumferential strain rates at the end of the follow-up were -4.2 ± 0.65 (AAMs patch), -3.5 ± 0.90 (ECM patch), -2.3 ± 0.45 (MI), and -4.5 ± 0.55 (Sham), and the corresponding AUC values for the circumferential strain rate were 11.7 ± 1.98 (AAMs patch), 7.9 ± 1.27 (ECM patch), 5.9 ± 1.56 (MI), and 13.31 ± 1.88 (Sham). Again, the AAMs patch group demonstrated better recovery.

Longitudinal strain showed no decline in either of the patch groups, and only the MI group against the Sham group showed significant decrease ([Figure 2D](#)). Longitudinal strain values at the 8-week time-point were -13.4 ± 2.16 (AAMs patch), -16.6 ± 2.83 (ECM patch), -12.9 ± 4.05 (MI), and -14.4 ± 2.41 (Sham), with the corresponding AUC values of 81.8 ± 22.23 (AAMs patch), 69.1 ± 10.87 (ECM patch), 56.1 ± 15.65 (MI), and 109.4 ± 12.67

(Sham) ([Figure 2E](#)). Longitudinal strain rate values at the 8-week time-point were -5.0 ± 0.63 (AAMs patch), -5.2 ± 0.86 (ECM patch), -4.2 ± 0.97 (MI), and -4.8 ± 0.40 (Sham), with the corresponding AUC values of 31.3 ± 6.88 (AAMs patch), 21.2 ± 2.67 (ECM patch), 17.2 ± 6.00 (MI), and 33.8 ± 5.12 (Sham).

Atrial natriuretic peptide expression

Atrial natriuretic peptide (*Anp*) mRNA expression ([Figure 2F](#)) was significantly lesser in both patch groups (3.6 ± 1.24 for AAMs and 2.3 ± 0.41 for ECM) than the expression in the MI group (7.9 ± 1.70). The possible presence of *Anp*-expressing AAMs may raise *Anp* mRNA levels in the AAMs patch group.

Fibrosis

Build-up of fibrous tissue was analyzed by the scar transmural index (scar thickness divided by the wall thickness at measurement point; [Figure 3A](#)) and ventricular wall thickness ([Figure 3B](#)). The mean scar transmural index values were $50.2\% \pm 3.69$ percentage points (AAMs patch), $53.1\% \pm 3.54$ percentage points (ECM patch), and $81.3\% \pm 4.26$ percentage points (MI), with the least fibrosis in the AAMs patch group. The mean ventricular wall thicknesses were 0.21 ± 0.01 cm (AAMs patch), 0.16 ± 0.08 cm (ECM patch), 0.061 ± 0.071 cm (MI), and 0.15 ± 0.094 cm (Sham). The greater thickness in the AAMs patch group can be attributable to the transplanted micrografts. The AAMs group also had the lowest degree of scar dispersion by planimetry ([Figure 3C](#)), although both patch groups were significantly different from the MI group. The mean scar dispersions were $51.4 \pm 13.7^\circ$ (AAMs patch), $59.4 \pm 14.1^\circ$ (ECM patch), and $152.4 \pm 9.0^\circ$ (MI). Moreover, the spread of epicardial patch was $135.3 \pm 4.7^\circ$ in the AAMs patch and $161.7 \pm 12.8^\circ$ in the ECM patch group. [Figure 3D](#) shows representative histological images from each group.

Endocardial interstitial fibrosis

Overall, the degree of tissue fibrosis in endocardial myocardium was lower in both patch groups than in the MI group. The endocardial area is the least tolerant to hypoxia and is the first region to be damaged and scarred after an ischemic insult. Evaluation of the endocardial fibrosis with collagen sub-type characterization is presented in [Figure 4](#). In all analyses, both patch groups demonstrated significantly lesser fibrosis than the MI group. The mean content of collagen fibers was $3.23\% \pm 0.83$ percentage points (AAMs patch), $1.67\% \pm 0.55$ percentage points (ECM patch), and $15.2\% \pm 1.96$ percentage points (MI); bright fibers were $0.035\% \pm 0.013$ percentage points (AAMs patch), $0.005\% \pm 0.002$ percentage points (ECM patch), and $0.309\% \pm 0.088$ percentage points (MI); green fibers were $0.77\% \pm 0.19$ percentage points (AAMs patch), $0.28\% \pm 0.062$ percentage points (ECM patch), and $4.54\% \pm 0.65$ percentage

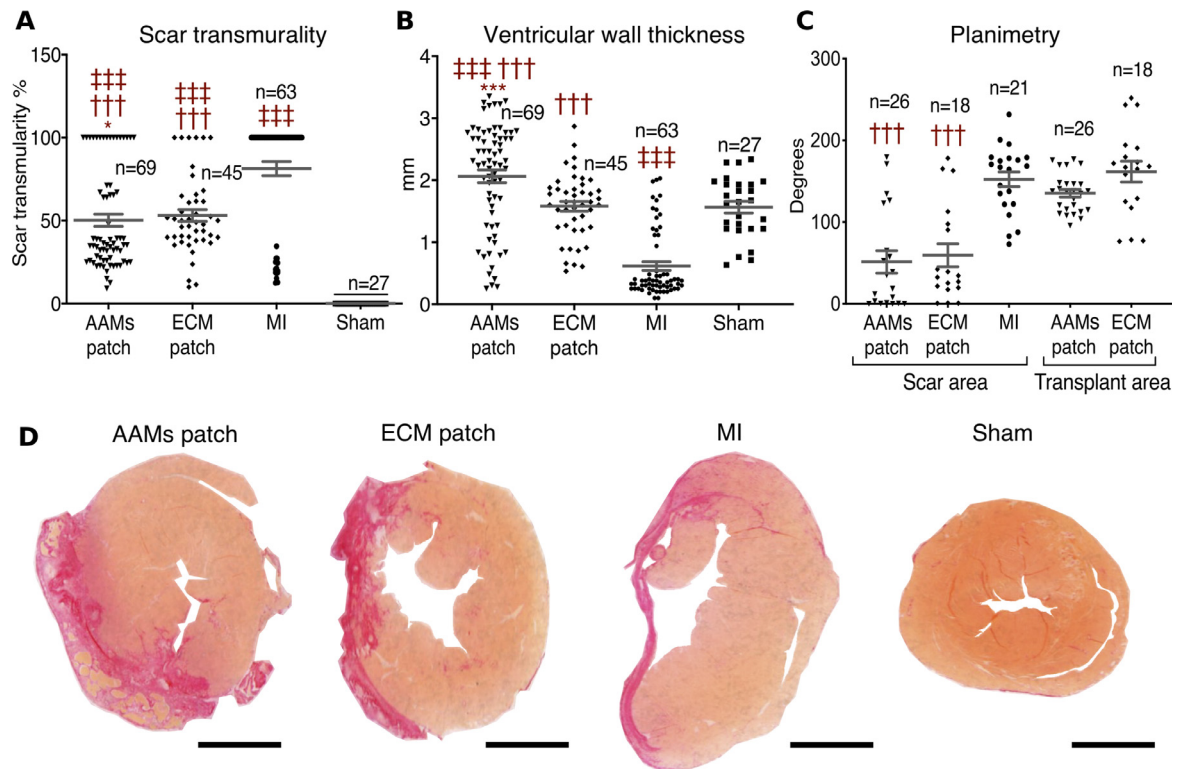


Figure 3 Ventricular morphometry. (A) Infarction scar transmurality assessed by measuring the thickness of the ventricular wall. (B) Ventricular wall thickness; thickness of the transplant was included in the measurement. (C) Planimetry analysis of the infarction scar angle. (D) Representative sections of Picosirius red-stained tissue samples assessed for tissue morphometry and infarction scar transmurality. Scale bar = 2 mm. */†‡ p-value < 0.05, **/††‡‡ p-value < 0.01, ***/†††† p-value < 0.001; *, p-value vs ECM patch group, †, p-value vs MI group, ‡, p-value vs the Sham group. Two-tailed Mann-Whitney *t*-test was applied, and data normality was assessed with the Shapiro-Wilk test for normality. From each heart sample, 3 adjacent histological sections were cut for analysis. The n-values represent total measurement sites assessed with high confidence (A and B, 9 measurements; C, 3 measurements/sample). ECM, extracellular matrix; MI, myocardial infarction.

points (MI); and orange fibers were $2.43\% \pm 0.65$ percentage points (AAMs patch), $1.38\% \pm 0.53$ percentage points (ECM patch), and $10.32\% \pm 1.32$ percentage points (MI).

Myocardium immunohistochemistry

We evaluated the preservation of myocardial tissue with anti-cTnT immunohistochemistry (Figure 5A and B) and by quantifying the picosirius red-negative area (Figure 5C and D). The area of cTnT-positive tissue in the sub-transplant area was larger in both patch groups than in the MI group. However, some MI-induced damage was observable across all interventional groups against the Sham group. cTnT-positive tissue in the sub-transplant encompassed $49.4\% \pm 1.94$ percentage points (AAMs patch), $53.6\% \pm 2.46$ percentage points (ECM patch), $35.0\% \pm 2.28$ percentage points (MI), and $99.68\% \pm 3.52$ percentage points (Sham). Within the site of infarction, significantly more picosirius red-negative nodules were found in the AAMs patch group than in the ECM patch or MI groups (Figure 5C). Non-collagenous nodule amounts were 3.6 ± 0.71 (AAMs patch), 0.7 ± 0.28 (ECM patch), and 1.1 ± 0.24 (MI). The nodules observed in the AAMs patch group were also the significantly largest compared with those

observed in the other groups (Figure 5C). The mean picosirius red-negative tissue area encompassed $1,205 \pm 258$ pixels (AAMs patch), 141 ± 49 pixels (ECM patch), and 258 ± 75 pixels (MI) (Figure 5D). These nodules remained cTnT-negative (Figure 5B), suggesting that they do not represent contractile cardiac tissue. Figure 5E presents the representative histological sections from each study group stained against cTnT.

Proteomics

In a separate experiment designed to compare AAMs and ECM patch molecular tissue-level responses with the same MI model and the 8-week follow-up, label-free site-targeted proteomics was performed on samples from the following areas: (1) ECM or AAMs patch (transplant), (2) sub-transplant, and (3) distal septal myocardium (Figure 1). We aimed to specifically dissect the therapeutic effect of AAMs from that of the ECM patch. All quantified and differentially expressed proteins (DEPs) are presented in Supplementary Material Data File S1 online, and the proteomics data have been uploaded to the mass spectrometry interactive virtual environment for in-depth review (Supplementary Material online). The quantified proteins (1,005 in

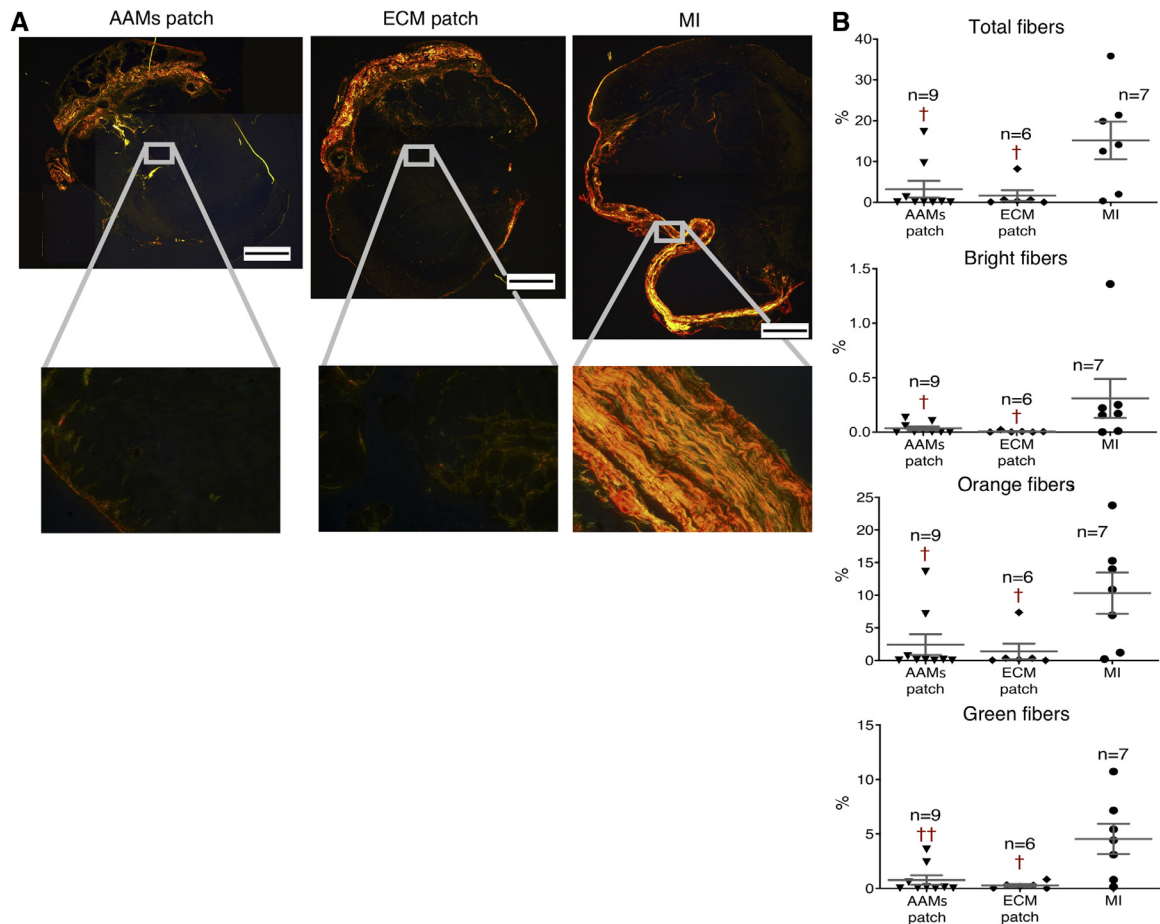


Figure 4 Evaluation of fibrosis. (A) Illustration of collagen analysis. Upper pictures are representative illustrations of the cardiac tissue sections photographed with circularly polarized light. Lower magnified and representative images were obtained from the endocardial surface of the infarction area from the left ventricle using $\times 40$ magnification. Scale bar = 1 mm. (B) Quantitation analysis of collagen fiber sub-populations from the endocardium. The uppermost panel shows the total content of Picrosirius Red-positive fibers in the analyzed tissue samples, whereas the panels below present the amount of the birefringent, orange, and green fibers seen with circularly polarized light, respectively below. Using Picrosirius Red staining and circularly polarized light, thinner Type-III fibers appeared green, whereas thicker and more mature Type-1 fibers appeared red or yellow. $*/\dagger/\ddagger p$ -value < 0.05 , $**/\dagger\dagger/\ddagger\ddagger p$ -value < 0.01 , $***/\dagger\dagger\dagger/\ddagger\ddagger\ddagger p$ -value < 0.001 ; $*$, p -value vs ECM patch group, $\dagger\dagger$, p -value vs MI group, \ddagger , p -value vs the Sham group. Two-tailed Mann-Whitney t -test was applied, and data normality was assessed with the Shapiro-Wilk test for normality. The scatter plot data represent mean \pm SEM. The n -values represent pooled sample means measured with high confidence. Each mean consists of 7 endocardial measurements and represents a separate heart sample. ECM, extracellular matrix; MI, myocardial infarction; SEM, standard error of the mean.

total) were assessed utilizing a Spearman correlation heatmap, which confirmed site-specific dissection of the transplant, sub-transplant, and remote septal samples. Samples from the patch transplant area clustered as a separate group, whereas the myocardial samples from the sub-transplant and septal areas formed another major cluster. Within this myocardial cluster, samples from the AAMs patch-treated group from both sub-transplant and septal areas clustered separately from the ECM patch samples without micrograft therapy, suggesting a wide-spread independent therapeutic effect of AAMs (Supplementary Material Figure S2 online). By comparing the AAMs patch group with the ECM patch controls, we identified 293 DEPs (45 upregulated and 248 downregulated) in the transplant area. In the sub-transplant area, 216 DEPs were characterized (151 upregulated and 65 downregulated), whereas in the septal area, 43 DEPs were identified (42 upregulated and 1 downregulated). All DEPs

were scrutinized using Ingenuity Pathway Analysis software to reveal associated canonical pathways, biologic functions, and disease states.

Transplant/patch zone: DEPs associated with the pathways for oxidative phosphorylation (activation), actin cytoskeleton signaling (activation), and sirtuin and calcium signaling (inactivation) were altered in the transplant zone of micrograft-treated vs non-treated tissue (Figure 6A). In transplant, the diseases and functions feature revealed processes related to the survival of cells and tissues. Specifically, functional categories including cell death and necrosis were significantly downregulated (B-H z-scores [Benjamini-Hochberg]: -2.99 and -3.43, respectively; Figure 6B), whereas those related to cell survival and cell viability were upregulated (B-H z-scores: +3.09 and +3.36, respectively; Figure 6B).

Subtransplant zone: Pathways related to cytoskeletal changes and reorganization were activated in the AAMs

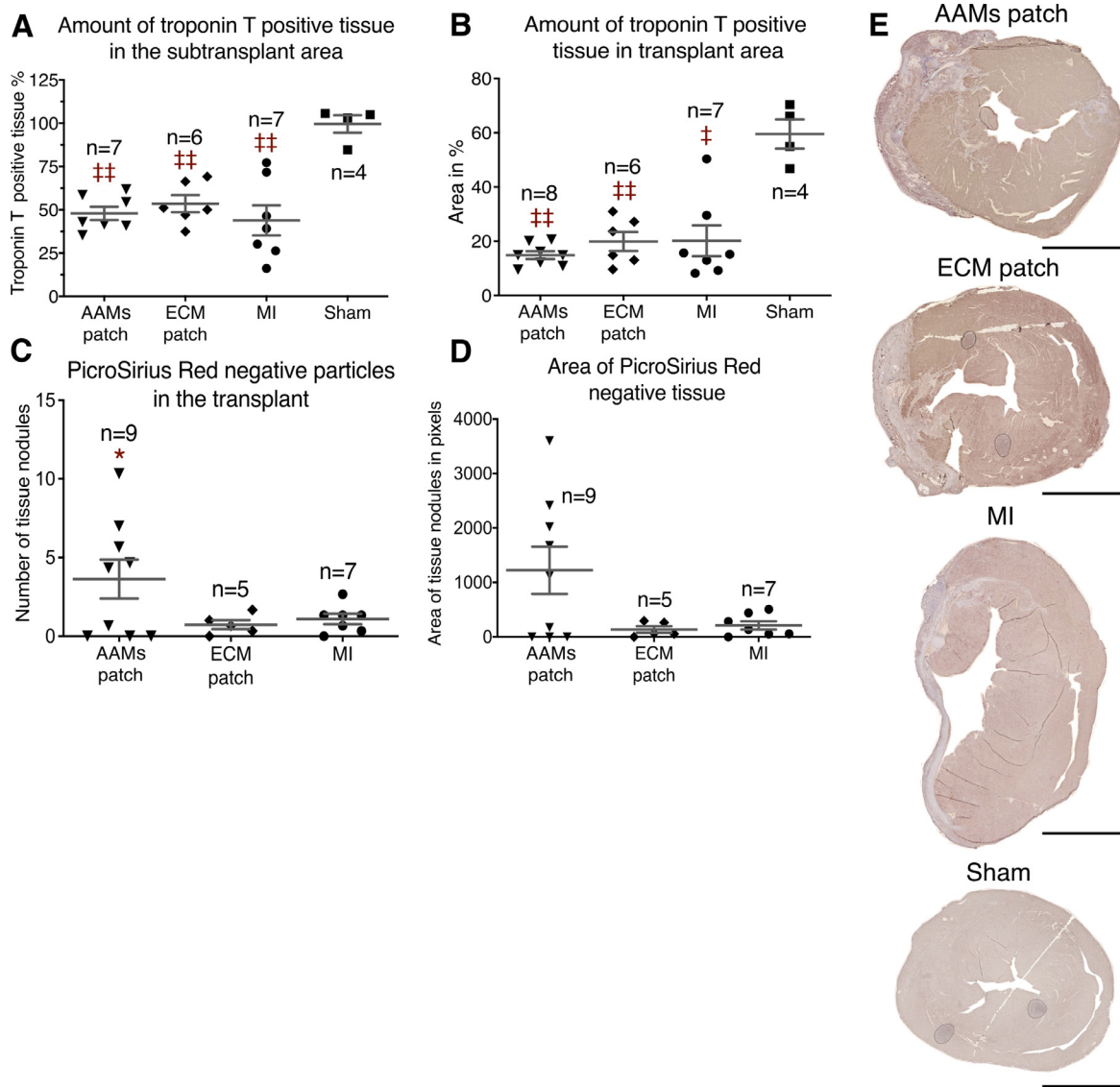


Figure 5 Histological preservation of myocardium. (A) Quantitation of troponin T-positive tissue content in the adjacent myocardium to the transplant and the sub-transplant zone. (B) Similarly, quantitation of anti-troponin T-positively stained area in the transplant. (C) Number of non-fibrous tissue nodules larger than 100 pixels inside the infarction scar (or the transplant area in AAMs and ECM patch groups) in the Picrosirius red-stained samples. (D) Area of non-fibrous, Picrosirius Red-negative tissue nodules. MI group values are presented as a reference. Reference values from the viable ventricular wall tissue (Sham) and the infarction scar (MI) are also presented in the graph. (E) Selected representative sections from the immunohistochemical staining set with anti-troponin T antibody. Scale bar = 2 mm. */†/‡ p-value < 0.05, **/††/‡‡ p-value < 0.01, ***/†††/‡‡‡ p-value < 0.001; *, p-value vs ECM patch group, †, p-value vs MI group, ‡, p-value vs the Sham group. Two-tailed Mann-Whitney *t*-test was applied, and data normality was assessed with the Shapiro-Wilk test for normality. The scatter plot data represent mean \pm SEM. The n-values represent pooled sample means measured with high confidence. Each mean consists of 7 endocardial measurements and represents a separate heart sample. AAM, atrial appendage micrograft; ECM, extracellular matrix; MI, myocardial infarction; SEM, standard error of the mean.

patch-treated sub-transplant zone: regulation of actin-based motility by Rho, RhoA signaling, and actin cytoskeleton signaling (Figure 6A). From a metabolic perspective, oxidative phosphorylation was significantly decreased, whereas glutathione redox reaction I was significantly altered, with increased expression of enzymes GPX3, GPX1, and glutathione S-transferase mu 2 (GSTM2) in the AAMs patch-treated group (Figure 6A; Supplementary Material online). Notably, functions related to muscle cell, especially cardiomyocyte, viability, and new muscle formation (formation

of muscle [B-H z-score: +2.80], differentiation of muscle and muscle cells [B-H z-score: +1.90], and apoptosis and death of muscle cells [B-H z-score: -1.91 and -1.92, respectively]) were significantly activated (Figure 6B). The inflammatory response (inflammation of organ [B-H z-score: -2.367]) and oxidative stress (B-H z-score: -2.236) showed decreased activity in the AAMs patch-treated group compared with that in the ECM patch group (Figure 6B). Interestingly, we found a 1.518-fold increase in the expression level of matricellular protein periostin (POSTN) and

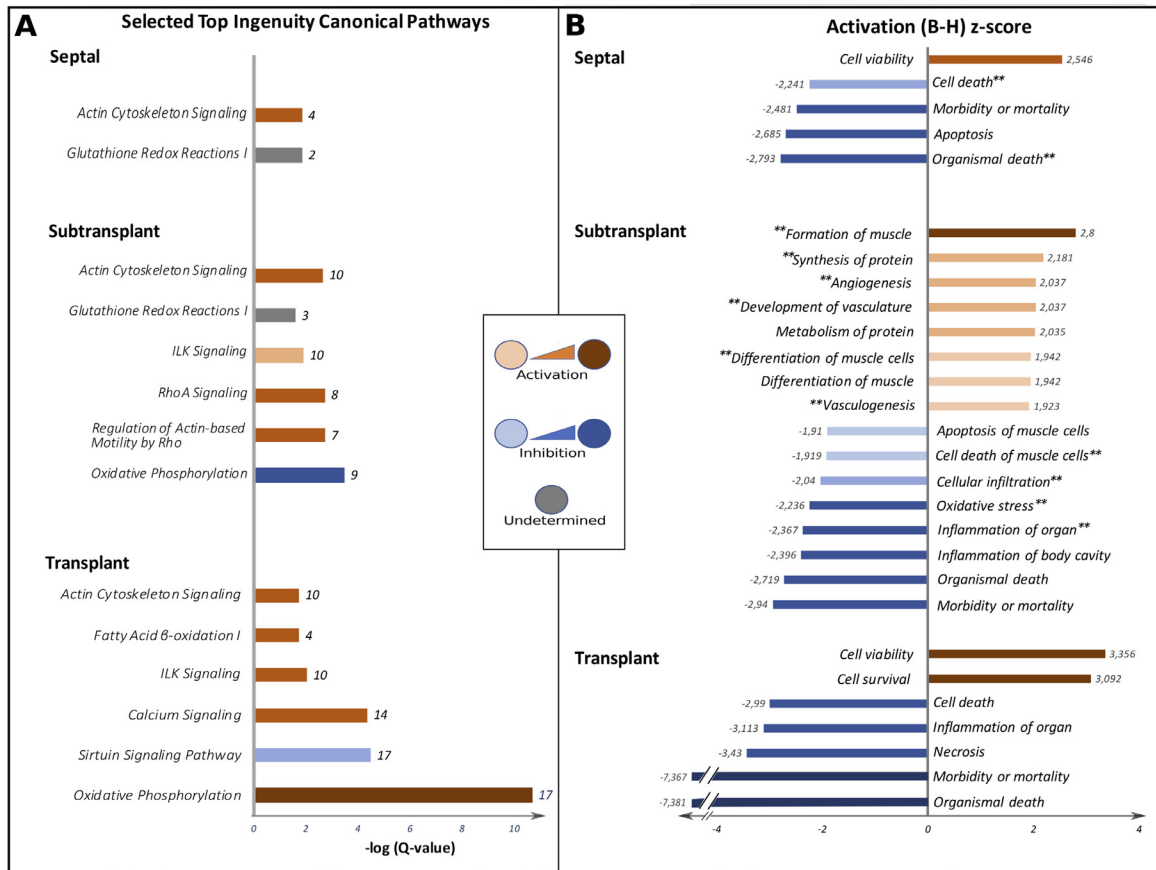


Figure 6 Proteomics, canonical pathways, and biologic functions. From each anatomic site, selected (A) canonical pathways and (B) functions are shown. The results are based on the IPA Software analysis of given representative locational DEPs (shown in Supplementary Data File S1 available online). The Q-value represents the B-H p -value. Q-value ≥ 1.5 and z -score ≥ 2 were used as criteria for significant activation or inactivation of a given pathway or process. All detected changes were compared with the ECM patch group; thus, these changes were attributed to AAMs transplantation. At the end of each bar in the sub-plot (A) is the number of DEPs associated with a given pathway, whereas in (B), the approximate z -score values are presented. Functions annotated with double asterisks are shown further in Figure 7. All canonical pathways as well as diseases and functions identified in each anatomic site are provided in Supplementary Material Figures S3 and S4 available online, respectively. AAMs, atrial appendage micrografts; B-H, Benjamini-Hochberg corrected p -value; DEPs, differentially expressed proteins; IPA, Ingenuity Pathway Analysis.

1.663-fold overexpression of tissue transglutaminase 2 enzyme (TGM2) with AAMs transplantation (Figure 7; Supplementary Material online). These protein-level changes provide molecular-level insight into the AAMs' therapeutic mechanism of action.

Septal zone: Similar to the sub-transplant area, actin cytoskeleton signaling and RhoA signaling pathways were predicted to be activated by the AAMs. Glutathione redox reactions I, with increased expression levels of GPX3 and GSTM2 enzymes, were also significantly altered (Figure 6A; Supplementary Material online). In the AAMs patch group, functions related to a dominant prosurvival effect in remote septum were increased. At the cellular level, cell viability was predicted to be activated (z -score: +2.546), whereas cell death and apoptosis were decreased (z -scores: -2.241 and -2.685, respectively; Figure 6B). At the system level, the functions morbidity or mortality and organismal death were predicted to be decreased (z -scores: -2.481 and -2.793, respectively; Figure 6B). Notably, overexpression of both matricellular protein POSTN (1.852-fold) and TGM2

enzyme (1.996-fold) were also detected here following AAMs transplantation, suggesting a wide-spread therapeutic effect (Figure 7).

All associated canonical pathways, biologic functions, and disease states are presented in Supplementary Material Figures S3 and S4 online. Supplementary Material Table S2 online further presents all associated DEPs to each canonical pathway, biologic function, and disease state.

Immunohistochemistry and quantitative real-time reverse transcription polymerase chain reaction

To qualitatively assess the expression of selected DEPs that were identified, we performed immunohistochemical staining for POSTN, TGM2, and GPX1 (Figure 8A). POSTN expression localized specifically to the extracellular space of the scar-myocardium interphase, mostly in the sub-transplant area. This kind of spatial staining pattern is well in line with the earlier reports on POSTN expression in the

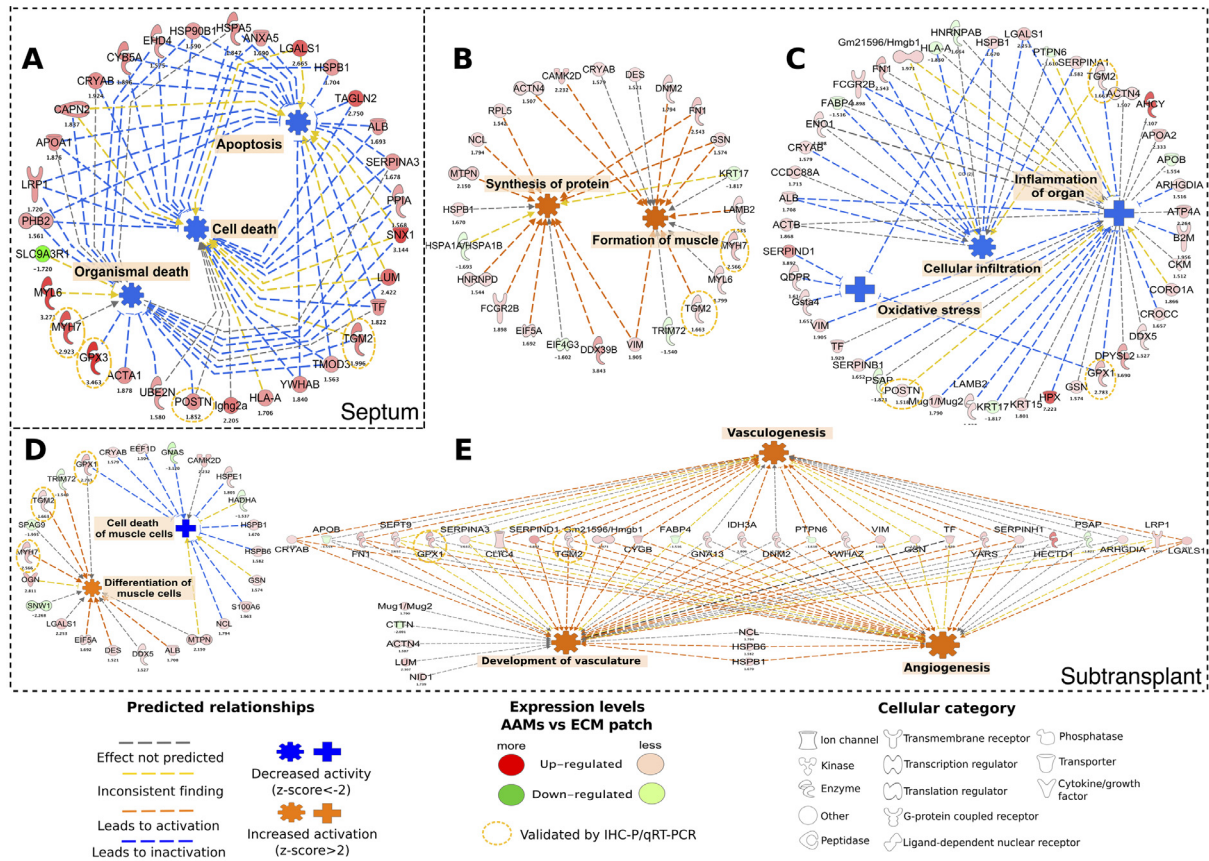


Figure 7 DEPs and associated biologic functions. Selected biologic functions from Figure 6 and associated DEPs are shown here. (A) Prosurvival functions and associated DEPs from the remote septum are presented. Periostin is documented cardiomyocyte mitogen and repair mediator after ischemic cardiac damage. (B) Functions related to anabolic protein and muscle metabolism from the sub-transplant are shown. Desmin is a pivotal intermediate filament in cardiomyocytes, whereas myosin 7 is a major slow-twitch myosin isoform in the heart. (C) DEPs associated with a decreased inflammatory reaction in the sub-transplant are shown. Glutathione peroxidase 1 is a ubiquitous enzyme with anti-oxidant properties catalyzing the hydrolysis of hydrogen peroxide radicals to water. (D) DEPs associated with increased cardiomyocytes differentiation in the sub-transplant immediately next to AAMs patch transplantation are shown. However, these functions showed only substantially strong trends toward activation or inactivation with a z -score = 1.9 for both functions (with the criterion for significant activation or inactivation being a z -score ≥ 2.0). (E) Functions related to angiogenesis with associated DEPs in the sub-transplant are shown. Transglutaminase 2 catalyzes the crosslinking of proteins and is associated with apoptosis. It is also documented to be a prosurvival factor for cardiomyocytes following ischemic insult. Small numeric counts below each DEP represent the expression ratio in the AAMs patch group divided by that of the ECM patch group. Statistical significance for differential protein expression was assessed using two-way ANOVA with p -value criterion ≤ 0.05 . AAMs, atrial appendage micrografts; ANOVA, analysis of variance; DEPs, differentially expressed proteins; ECM, extracellular matrix.

heart after acute MI.¹⁶ In contrast, TGM2 expression mainly localized to the patch and intracellular compartment of the cardiomyocytes near the minor scar areas, whereas GPX1 expression showed less pronounced staining but localized in the myocardium to the cardiomyocytes near the scar areas and vascular walls and more intense in the patch areas. Results from quantitative real-time polymerase chain reaction confirmed overexpression for *Postn*, *Myh7*, and *Gpx3* in both sub-transplant and septal zones (Figure 8B). The mRNA expression levels for *Postn*, *Myh7*, and *Gpx3* were significantly higher in the AAMs patch group than the Sham ($p = 0.010$, 0.014 , and 0.028 , respectively). Moreover, the expression of *Gpx3* was higher in the AAMs patch than in the ECM patch group ($p = 0.046$). *Tgm2* mRNA levels did not show significant changes between groups. When comparing the gene and protein expression results, it is important to consider the substantial differences and

variation in biologic regulation and temporal dynamics between transcription and translation.¹⁷

Discussion

In a murine model of MI and HF, epicardial patch therapy demonstrated significantly improved cardiac function, greatly preserved myocardial structure, attenuated ventricular wall scarring, and dramatically restricted tissue damage. Myocardial site-targeted proteomics revealed the selective cell and molecular-level therapeutic effects of AAMs. These included activation of cardiomyogenesis, angiogenesis and anti-inflammation pathways, as well as reduction of oxidative stress.

Cell-based therapies have long been investigated for their ability to deliver regenerative effects. Atrial appendages act as niches for cardiac progenitor cells and serve as

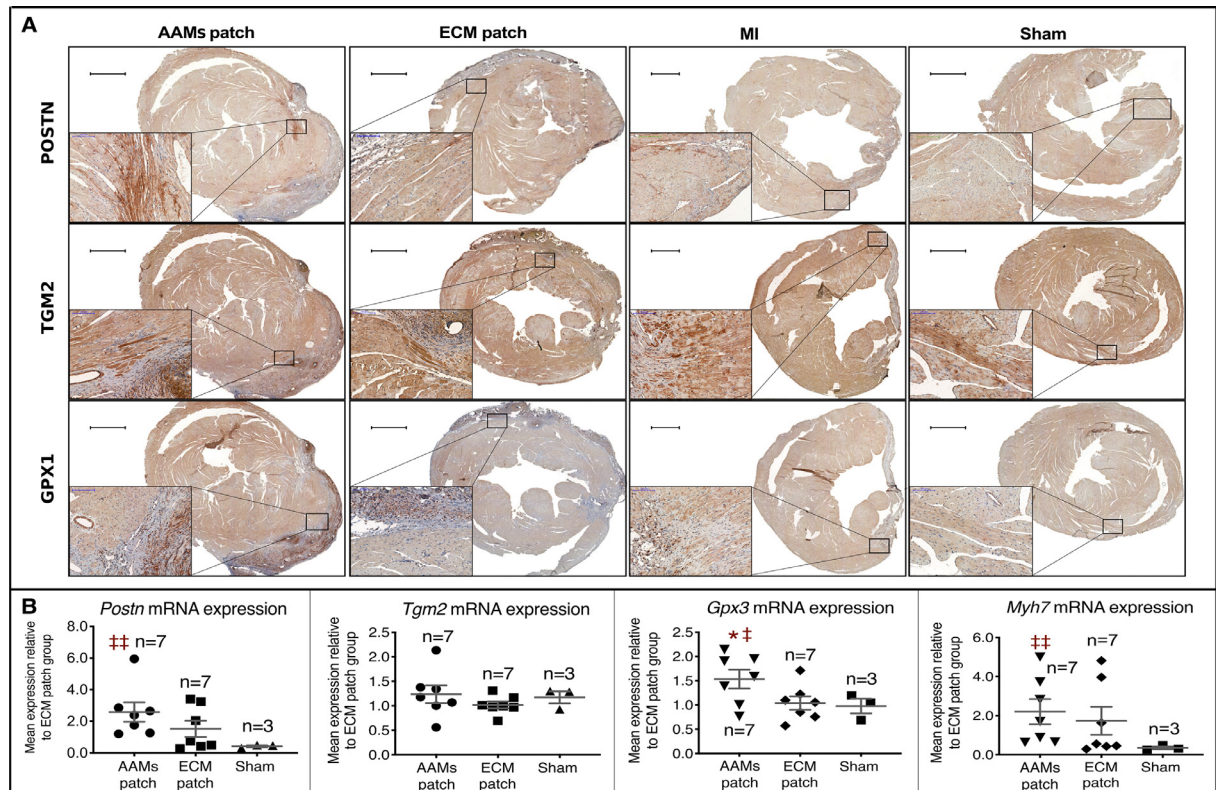


Figure 8 Validative IHC-P and qRT-PCR analysis. The set of samples preserved in paraffin was for evaluating the fibrotic content and overall histomorphology of the study groups by IHC-P. Assessment by qRT-PCR was applied for the same set of cryopreserved samples as in the quantitative proteomics. (A) The representative images with magnifying sub-captions from the IHC-P stainings are presented here for 3 selected proteins of interest: POSTN, TGM2, and GPX1 (n = 4 for each). POSTN exhibited marked expression in the patch zone as well as in the extracellular interphase of fibrotic scar areas and myocardium in all groups. TGM2 expression was mainly localized to the intracellular compartment of cardiomyocytes and endothelial cells, with the most pronounced expression localizing to cardiomyocytes with immediate contact with the fibrotic areas in the sub-transplant zone right below the patch. Finally, the GPX1 exhibited marked expression in the patch itself and in the vascular wall. Intracellular expression in cardiomyocytes seemed to be more pronounced in the AAMs group as compared with the ECM group. The black scale bar = 1000 μ m, green scale bar = 200 μ m, and blue scale bar = 100 μ m. (B) The results of the qRT-PCR. Transcription of *Myh7*, *Gpx3*, and *Postn*, together with the production of the corresponding mRNAs, was significantly higher after AAMs patch transplantation (n = 7) in comparison with the ECM patch transplantation (n = 7) when both were compared against the steady-state gene expression represented by the Sham expression levels (n = 3). *Tgm2* mRNA expression was not altered. */† p-value < 0.05, **/†† p-value < 0.01, *, p-value vs ECM patch group, †, p-value vs Sham group. The p-values were calculated using a one-way unpaired t-test with Welch's correction for unequal variances. The normality of the data was assessed with the Shapiro-Wilk normality test. The scatter plot data represent mean \pm SEM. The n-values represent separate heart cryo samples measured with high confidence (1 cryo sample/individual). AAMs, atrial appendage micrografts; ECM, extracellular matrix; GPX1, glutathione peroxidase 1 protein; *Gpx3*, glutathione peroxidase 3 mRNA; IHC-P, immunohistochemistry on paraffin-embedded tissues; *Myh7*, myosin heavy chain 7 mRNA; POSTN/*Postn*, periostin (protein/mRNA); qRT-PCR, quantitative real-time reverse transcription polymerase chain reaction; SEM, standard error of the mean; TGM2/*Tgm2*, transglutaminase 2 (protein/mRNA).

a rational autologous source of myocardial tissue for therapy owing to their easy accessibility and relative redundancy for cardiac function.^{11,12} We mechanically disaggregated the atrial appendage tissue after harvesting to yield micrografts ready for epicardial transplantation.¹⁸

Here, we utilized mass spectrometry-based quantitative proteomics to decipher myocardial site-specific responses to epicardial AAMs after MI. We demonstrated a widespread cardioprotective effect reaching from the sub-transplant myocardium to remote myocardial areas. In the sub-transplant area, decreased oxidative metabolism and oxidative stress with increased glutathione metabolism suggest an AAMs-induced change in metabolism toward glycolysis, a process associated with improved regeneration capacity in

multiple studies.^{19–23} We propose that AAMs induced, likely through a paracrine mechanism, a metabolic shift from oxidative to glycolytic metabolism in the ischemically challenged sub-transplant area and a preoperative microenvironment for surviving cardiomyocytes, ultimately setting the stage for functional recovery. This effect is further supported by our observation that functions such as formation of muscle and differentiation of muscle cells, were activated. Moreover, restoration of functional myocardial tissue is not merely a process of cardiomyocytes but necessitates the formation of new ECM, blood vessels, and lymphatics, all processes of which are mostly orchestrated by cell types other than cardiomyocytes. Our findings demonstrate increased angiogenesis, vasculogenesis, and wide-spread

prosurvival changes in the myocardium, which indicate induction of a protective and restorative myocardial environment by AAMs.

Increased expression of the cardiomyocyte mitogen and matricellular protein POSTN in both the sub-transplant and remote septal zones further clarifies the cellular and molecular mechanisms of AAMs patch transplantation. The secreted matricellular protein POSTN mediates cell-matrix interactions and repair after tissue injury.^{24,25} Our data support the association of POSTN expression and myocardial regenerative signaling through the Rho-kinase pathway.¹⁶ During tissue repair and healing after MI, POSTN is secreted to the cardiac interstitium by activated cardiac fibroblasts¹⁶ to stimulate cardiomyocyte cell cycle re-entry and prevent myocardial rupture after infarction.^{16,24}

In the sub-transplant myocardium, AAMs selectively increased expression of proteins associated with muscle formation, vasculature development, and glutathione metabolism. DEPs were also negatively associated with cellular infiltration. In both sub-transplant and septal myocardia, remote to the transplant site, we discovered increased expression of proteins associated with cardiomyocyte contraction, including MYH7, MYL1, MYL6, MYL12B, ACTA1, ACTN4, DES, and CAMK2D. Interestingly, the expression of proteins involved in glutathione metabolism and anti-oxidant defenses (GSTM2, GSTA4, GPX3) was also significantly increased in the sub-transplant and remote septal sites treated by AAMs patch therapy compared with those treated by ECM patch therapy without micrografts. The observed *Gpx3* gene expression difference between AAMs and ECM patch groups further strengthens this association of the AAMs mechanism of action through enhanced myocardial anti-oxidant defenses. In addition, we found a significant increase in cell viability and a significant decrease in cell death and apoptosis in the septal zone in AAMs patch-treated hearts. This prosurvival action is a documented paracrine effect of cardiac stem or progenitor cell therapy.²⁶

Interestingly, the AAMs treatment suppressed inflammatory reactions in the ischemia-challenged sub-transplant zone and increased angiogenesis. Proteins associated with muscle cell differentiation were also upregulated in this zone treated with AAMs. Thus, our results suggest that AAMs can modulate the inflammatory response following MI in a way that promotes functional myocardial recovery.

Although the AAMs selectively induced therapeutic myocardial signaling and protein expression after MI, our results indicate that the ECM patch itself also protects against experimental MI and fibrosis. As a mechanically supportive structure, the epicardial ECM patch can alter the biomechanics of the failing left ventricle beneficially. By increasing wall thickness, ECM patch transplantation can relieve tension in the myocardial wall and subsequently reduce oxygen demand. An epicardial ECM patch may also modify the mechanical force vectors along the ventricular wall to favor an energetically more beneficial contraction.

Although our study provides indirect insights into AAMs survival on the epicardial surface after MI, a targeted

evaluation of the extent of autologous graft survival utilizing AAMs-specific experimental long-term labeling methodologies would be required to unequivocally address the extent and duration of a graft survival. Interestingly, we however found abundant tissue nodules staining negative for collagen using picrosirius red. The higher expression of *Anp* mRNA that was observed in the transplant zone and apices of AAMs patch group relative to same areas in the ECM patch group can also indicate the persistence of the AAMs.

This study complements our previously reported first clinical application of autologous AAMs patch epicardial transplantation¹⁴ and the clinical open-label safety and feasibility trial (ClinicalTrials.gov identifier NCT02672163).¹⁵ Our results in this study provide insights into the mechanisms of action of epicardial AAMs patch transplantation and associate its therapeutic effects, reduced cardiac fibrosis, and preservation of functional myocardium with activation of pathways responsible for angiogenesis and cardiogenesis in the ischemically damaged myocardium. Contrary to the long-lasting trend of developing cardiac cellular therapies with increasing complexity, our results underscore the therapeutic possibilities of readily clinically applicable and straight-forward autologous procedures.

In conclusion, the therapeutic effect of the AAMs patch is mediated through multifaceted synergy among (1) mechanical support with ventricular unloading by the ECM patch transplantation, as demonstrated by improved ECHO parameters, attenuated fibrosis, and preservation of troponin T-positive myocardium in both acellular ECM patch- and AAMs patch-treated groups; (2) enhanced cardiomyocyte contractility through expression of proteins associated with contractile apparatus and Ca^{2+} signaling in the AAMs patch group; (3) enhanced reparative microenvironment through activated anaerobic glycolysis, angiogenesis, and cell viability; (4) decreased oxidative stress and enhanced anti-oxidant protection by increased glutathione metabolism; (5) upregulated cellular matrix mitogenic matricellular POSTN; and (6) modulated inflammation. These results provide a molecular basis for epicardial AAMs patch transplantation therapy in ischemic HF for myocardial rescue and repair.

Disclosure statement

None of the authors has a financial relationship with a commercial entity that has an interest in the subject of the presented manuscript or other conflicts of interest to disclose.

Antonio Graziano, a manuscript non-author member of the Advanced Alcohol and Drug Counselor consortium, is the founder of and owns stock in Human Brain Wave Srl, manufacturer of the Rigenera Human Brain Wave tissue processor.

The authors thank Päivi Leinikka for her invaluable help in carrying out the animal experiments, Lahja Eurajoki and Nada Bechara-Hirvonen for their expert laboratory assistance, and Sole Lätti for the illustrations. Tissue processing was carried out at the Tissue Preparation and Histochemistry Unit of the Faculty of Medicine, University of Helsinki,

Finland. Scanning of histological sections on slides was carried out at the Digital Microscopy and Molecular Pathology Unit, Institute for Molecular Medicine Finland, Helsinki, Finland. Proteomics analyses were performed at the Meilahti Clinical Proteomics Core Facility, University of Helsinki, Finland, supported by Biocenter Finland, Helsinki, Finland.

This work was supported by Finnish Funding Agency for Technology and Innovation (3137/31/2013, E.K.), Finnish state research funding for expert responsibility area (TYH215311/M.K., TYH2012203/A.H.), Academy of Finland (275882/E.M.), and Finnish Foundation for Cardiovascular Research (2016/E.M.).

Supplementary data

Supplementary data associated with this article can be found in the online version at www.jhltonline.org/.

Supplementary materials

Supplementary material associated with this article can be found in the online version at <https://doi.org/10.1016/j.healun.2020.03.023>.

References

1. GBD 2015 Mortality and Causes of Death Collaborators. Global, regional, and national life expectancy, all-cause mortality, and cause-specific mortality for 249 causes of death, 1980-2015: a systematic analysis for the Global Burden of Disease study 2015. *Lancet* 2016;388:1459-544.
2. Thygesen K, Alpert JS, Jaffe AS, et al. Fourth universal definition of myocardial infarction (2018). *Circulation* 2018;138:e618-51.
3. Braunwald E. Heart failure. *JACC Heart Fail* 2013;1:1-20.
4. Desta L, Jernberg T, Löfman I, et al. Incidence, temporal trends, and prognostic impact of heart failure complicating acute myocardial infarction. The SWEDHEART Registry (Swedish web-system for enhancement and development of evidence-based care in heart disease evaluated according to recommended therapies): a study of 199,851 patients admitted with index acute myocardial infarctions, 1996 to 2008. *JACC Heart Fail* 2015;3:234-42.
5. Lampinen M, Vento A, Laurikka J, et al. Rational autologous cell sources for therapy of heart failure - vehicles and targets for gene and RNA therapies. *Curr Gene Ther* 2016;16:21-33.
6. Hashimoto H, Olson EN, Bassel-Duby R. Therapeutic approaches for cardiac regeneration and repair. *Nat Rev Cardiol* 2018;15:585-600.
7. Fisher SA, Brunskill SJ, Doree C, Mathur A, Taggart DP, Martin-Rendon E. Stem cell therapy for chronic ischaemic heart disease and congestive heart failure. *Cochrane Database Syst Rev* 2014;4:CD007888.
8. Messina E, De Angelis L, Frati G, et al. Isolation and expansion of adult cardiac stem cells from human and murine heart. *Circ Res* 2004;95:911-21.
9. Meilhac SM, Buckingham ME. The deployment of cell lineages that form the mammalian heart. *Nat Rev Cardiol* 2018;15:705-24.
10. Koninckx R, Daniëls A, Windmolders S, et al. The cardiac atrial appendage stem cell: a new and promising candidate for myocardial repair. *Cardiovasc Res* 2013;97:413-23.
11. Leinonen JV, Emanuelov AK, Platt Y, et al. Left atrial appendages from adult hearts contain a reservoir of diverse cardiac progenitor cells. *PLoS One* 2013;8:e59228.
12. Detert S, Stamm C, Beez C, et al. The atrial appendage as a suitable source to generate cardiac-derived adherent proliferating cells for regenerative cell-based therapies. *J Tissue Eng Regen Med* 2018;12:e1404-17.
13. Fanton Y, Houbrechts C, Willems L, et al. Cardiac atrial appendage stem cells promote angiogenesis in vitro and in vivo. *J Mol Cell Cardiol* 2016;97:235-44.
14. Lampinen M, Nummi A, Nieminen T, Harjula A, Kankuri E, Consortium AADC. Intraoperative processing and epicardial transplantation of autologous atrial tissue for cardiac repair. *J Heart Lung Transplant* 2017;36:1020-2.
15. Nummi A, Nieminen T, Pätälä T, et al. Epicardial delivery of autologous atrial appendage micrografts during coronary artery bypass surgery-safety and feasibility study. *Pilot Feasibility Stud* 2017;3:74.
16. Frangogiannis NG. Matricellular proteins in cardiac adaptation and disease. *Physiol Rev* 2012;92:635-88.
17. Zhang B, Wang J, Wang X, et al. Proteogenomic characterization of human colon and rectal cancer. *Nature* 2014;513:382-7.
18. Trovato L, Monti M, Del Fante C, et al. A new medical device Regeracons allows to obtain viable micro-grafts from mechanical disaggregation of human tissues. *J Cell Physiol* 2015;230:2299-303.
19. Lalowski MM, Björk S, Finckenberg P, et al. Characterizing the key metabolic pathways of the neonatal mouse heart using a quantitative combinatorial omics approach. *Front Physiol* 2018;9:365.
20. Nakada Y, Canseco DC, Thet S, et al. Hypoxia induces heart regeneration in adult mice. *Nature* 2017;541:222-7.
21. Kimura W, Xiao F, Canseco DC, et al. Hypoxia fate mapping identifies cycling cardiomyocytes in the adult heart. *Nature* 2015;523:226-30.
22. Kimura W, Sadek HA. The cardiac hypoxic niche: emerging role of hypoxic microenvironment in cardiac progenitors. *Cardiovasc Diagn Ther* 2012;2:278-89.
23. Puente BN, Kimura W, Muralidhar SA, et al. The oxygen-rich postnatal environment induces cardiomyocyte cell-cycle arrest through DNA damage response. *Cell* 2014;157:565-79.
24. Kühn B, del Monte F, Hajjar RJ, et al. Periostin induces proliferation of differentiated cardiomyocytes and promotes cardiac repair. *Nat Med* 2007;13:962-9.
25. Chen Z, Xie J, Hao H, et al. Ablation of periostin inhibits post-infarction myocardial regeneration in neonatal mice mediated by the phosphatidylinositol 3 kinase/glycogen synthase kinase 3 β /cyclin D1 signalling pathway. *Cardiovasc Res* 2017;113:620-32.
26. Mirotsov M, Jayawardena TM, Schmeckpeper J, Gnecci M, Dzau VJ. Paracrine mechanisms of stem cell reparative and regenerative actions in the heart. *J Mol Cell Cardiol* 2011;50:280-9.